# Properties of Polyether–Polyurethane Block Copolymers: Effects of Hard Segment Length Distribution

**John A. Miller, Shaow B. Lin,† Kirk K. S. Hwang,‡ K. S. Wu,§ P. E. Gibson, and Stuart L. Cooper***

*Department of Chemical Engineering, University of Wisconsin, Madison, Wisconsin 53706.*
*Received September 2, 1983*

ABSTRACT: Two sets of polyether–polyurethane block polymers based on poly(tetramethylene oxide) (PTMO), 4,4′-methylenebis(phenyl isocyanate) (MDI), and butanediol (BD) were prepared in different ways to produce materials with equivalent stoichiometries but different hard segment length distributions. One set of materials was prepared by a one-step polymerization with butanediol as the chain extender. The second series was synthesized by a multistep method using butanediol and/or bis(4-hydroxybutyl) 4,4′-methylenebis(phenylcarbamate) (BMB) as the chain extender. The single-step polymers are shown to have fewer hard segments containing a single MDI unit than the corresponding multistep samples. The result of this is that the multistep materials exhibit a greater degree of phase mixing, as the very short hard segments are more likely to be dissolved in the soft phase than are longer hard segments. The evidence for this comes from the behavior of the sample ET-20M, an MDI/PTMO alternating copolymer. The hard phase volume fraction and crystallinity are greater in the single-step materials due to the lower degree of phase mixing in these polymers. The results of infrared spectroscopy, differential scanning calorimetry, dynamic mechanical analysis, stress–strain testing, and small-angle X-ray scattering are all shown to be consistent with the differences in hard segment length distributions and the differences in phase mixing which accompany the distributional differences.

## I. Introduction

Polyurethane block copolymers which consist of alternating flexible and rigid segments often possess a two-phase morphology due to segmental incompatibility. The factors which influence the phase separation include segmental polarity difference, segmental length, crystallizability of either segment, intra- and intersegment interactions such as hydrogen bonding, overall composition, and molecular weight. The elasticity, toughness, and other physical properties of these materials are determined largely by the size, crystallinity, and interconnectivity of the hard domains as well as the nature of the domain interface and the mixing of hard segments in the soft segment phase.

Seymour et al.[1-3] in an IR dichroism study of MDI/BD/PTMO-1000 (1000 MW PTMO) polyurethanes found that an increase in the hard segment content from 24 to 28 wt % MDI changed the hard segment domain microstructure from an isolated to an interconnected morphology. The hard segment content was increased by increasing the average hard segment length at fixed soft segment length. Abouzahr et al.[4] used wide-angle X-ray diffraction to study the crystal structure of MDI/BD/PTMO-2000 polyurethanes. These materials had the same chemical constituents as those studied by Seymour et al. but had longer segmental lengths. Abouzahr found no detectable crystalline diffraction for samples with less than 35 wt % MDI. On the basis of small-angle X-ray scattering and stress relaxation studies, Abouzahr et al. also proposed that polyurethanes have an interlocked domain morphology at moderate MDI content (35 and 45 wt %). Bonart[5,6] also examined the packing of MDI/BD hard segments using X-ray scattering and suggested that hard segments were laterally associated forming lamellae with a thickness limited by the average hard segment length. Using electron microscopy and X-ray diffraction analysis, Schneider et al.[7] proposed that the MDI/BD hard segment domain existed in a micelle-like structure which was made up of a lateral association of hard segment units. The hard segment units were aligned perpendicular to the fibril axis or radial direction in loosely organized spherulites. Recently, Van Bogart et al.,[8] on the basis of X-ray scattering and DSC studies, also concluded that MDI/BD hard segments exist in semicrystalline domains whose crystallinity increased as the hard segment length increased.

In an attempt to investigate the effect of segment size and polydispersity on hard segment crystallinity and material properties, Ng et al.[9] conducted a thorough characterization of piperazine/BD/PTMO-based polyurethanes which possessed a well-defined segment molecular weight and molecular weight distribution and no possibility for intermolecular hydrogen bonding. They found that copolymers with a narrow hard segment length distribution exhibited better microphase separation, higher modulus, and higher elongation at break than equivalent materials containing polydisperse hard segments. Previously, Harrell[10] reported that a hard segment consisting of two piperazine units extended by BD exhibited a sharp and distinct melting point at about 50 °C. The melting point of the family of piperazine-based polyurethanes increased as the hard segment length increased following Flory's equation[11] which predicts melting point variation with degree of polymerization. Harrell also reported that hard segments with one repeat unit cocrystallized with segments containing two repeat units but not with segments containing three or four repeat units. Samuels and Wilkes[12] also studied these materials and found that the WAXS peaks became sharper with increasing hard segment length, indicating an increasing hard segment lamellar thickness. While it appears much has been learned by the study of these piperazine-based polyurethanes, they are highly crystallizable non-hydrogen bonded systems which may not serve as an appropriate model for understanding the effects of segment polydispersity in MDI/BD polyurethanes. Therefore, it was deemed desirable to study the effect of hard segment length distribution on morphology and properties of MDI/BD/PTMO polyurethanes.

In the present study, several poly(tetramethylene oxide)-based polyurethanes with different hard segment length distributions were synthesized. The chemical composition of these materials is listed in Table I. We define a hard segment of MDI/BD/PTMO as follows: a

† Current address: Syntex Ophthalmics, Research and Development Laboratory, Phoenix, AZ.
‡ Current address: Life Science Sector Laboratory, 3M, St. Paul, MN.
§ Visiting Scholar, Shanghai Institute of Organic Chemistry, Shanghai, People's Republic of China.

0024-9297/85/2218-0032$01.50/0 

**Scheme I**

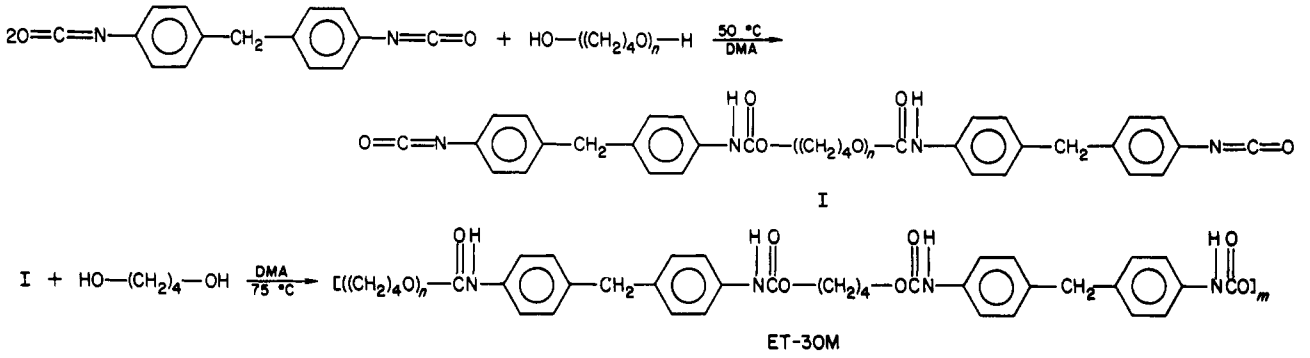

**Table I**
**Composition of Polyurethane Block Polymers[a–c]**

| sample | MDI:BD:PTMO molar ratios | MDI, wt % | hard segment wt fraction | MDI units per hard segment |
|---|---|---|---|---|
| ET-20M | 1:0:1 | 20 | 0.23 | 1 |
| ET-30M | 2:1:1 | 30 | 0.39 | ⟨2⟩ |
| ET-38M | 3:2:1 | 38 | 0.50 | ⟨3⟩ |
| ET-48M | 5:4:1 | 48 | 0.63 | ⟨5⟩ |
| ET-38S | 3:2:1 | 38 | 0.39 | ⟨3⟩ |
| ET-48S | 5:4:1 | 48 | 0.63 | ⟨5⟩ |

[a] The number-average molecular weight, $M_n$, of PTMO was 990. [b] As determined by GPC, the $M_n$'s of the block polymers were about $3 \times 10^4$, except for ET-20M which had an $M_n$ of about $5 \times 10^4$. [c] The hard segment weight fraction, $W$(HS), was calculated as follows for molar ratios of $x$:($x$ − 1):1 of MDI:BD:PTMO. Let $A$(SS) = MW(PTMO) − 2[MW(OH)] = 990 − 34 = 956, and $A$(HS) = $x$[MW(MDI)] + ($x$ − 1)[MW(BD)] + 2[MW(OH)] = 340$x$ − 56. Then $W$(HS) = $A$(HS)/[$A$(HS) + $A$(SS)] = (340$x$ − 56)/(340$x$ + 990).

hard segment of length $x$ is composed of $x$ MDI's, ($x$ − 1) BD's, and 2 OH's. Note that hard segments are terminated with planar (rigid) urethane groups and that the minimal hard segment length is one. Many hard segments of length one may be dissolved in the soft phase, but they are still designated as hard segments. One should not confuse the definition of "hard segment" with the concept of "hard domain". Samples designated with an M were synthesized in a multistep process that yielded a hard segment length distribution with a high fraction of single MDI unit segments. The materials designated with an S were made by a random single step polymerization in solution. The two sets of materials were produced at a fixed soft segment molecular weight, hence the hard segment weight fraction increases as the average length of the hard segments increases.

## II. Experimental Aspects

**A. Synthesis of Polyether–Polyurethane Block Copolymers. 1. Preparation of Reactants.** Poly(tetramethylene oxide) (PTMO) (Quaker Oats Co.) was dehydrated under a rough vacuum at 50 °C for 2 days. 4,4′-Methylenebis(phenyl isocyanate) (MDI) (Polysciences) was melted and pressure filtered under $N_2$ at 60 °C followed by recrystallization from hexane in an ice bath. Tetrahydrofuran (THF) (Aldrich), 1,4-butanediol (BD) (Aldrich), and *N,N*-dimethylacetamide (DMA) (Aldrich) were dried over calcium hydride for 2 days and then vacuum distilled. Methanol (Aldrich) was dehydrated with a Grignard reagent prior to distillation. Dimethyl sulfoxide ($Me_2SO$) (Aldrich) and hexane (Aldrich) were dried over 4-Å molecular sieves. Hexamethyldisilazane (Aldrich) and chlorotrimethylsilane (Aldrich) were used as received.

**2. Synthesis of Materials by the Multistep Method. a. ET-20M.** The polyether–polyurethane containing only one MDI unit for each hard segment was prepared by reacting equal moles of PTMO (990 MW) and MDI in DMA (20% w/v) at 75 °C with 0.15% stannous octoate catalyst. After the solution was stirred for 2 h, the polymer was precipitated and dried under vacuum.

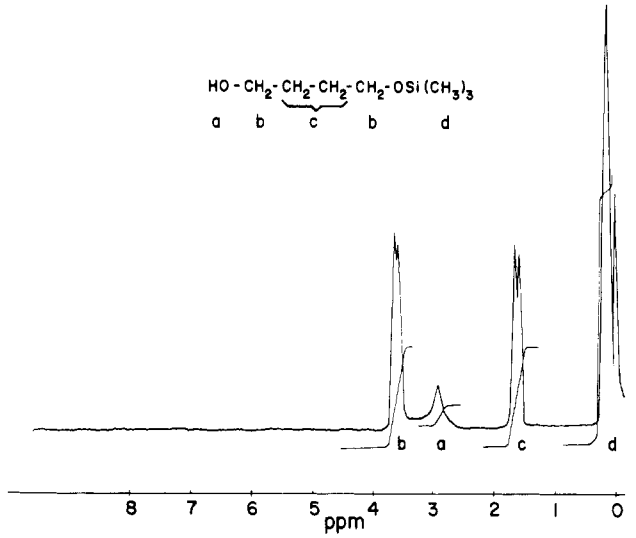


**Figure 1.** NMR spectrum of 4-(trimethylsiloxyl)-1-butanol.

ET-20M is included in the multistep series because all of the hard segments are one MDI unit in length. Compared to single step materials, the multistep materials have a higher fraction of hard segments which are one MDI unit in length. This difference is more fully discussed below.

**b. ET-30M.** The polyether–polyurethane containing two MDI units extended with one 1,4-butanediol (BD) species was prepared as described in reaction Scheme I.

Compound I was made by slowly adding a solution of 9.9 g (0.01 mol) of PTMO (990 MW) in 35 $cm^3$ of dry DMA to a solution of 5 g (0.02 mol) of MDI in 10 $cm^3$ of DMA and stirring for 1 h at 50 °C. This reaction condition allowed PTMO to be capped by MDI and resulted in a free N=C=O group at each chain end of this oligomer. The completion of this step of the reaction was verified by IR spectroscopy. It should be pointed out that compound I is not a pure species. Some higher degree of linking occurs to produce longer oligomers and hence a final polymer with a distribution of hard segment sequence lengths. Later in the discussion of the sequence length distribution the exact distribution will be calculated. Scheme I illustrates the average products obtained.

ET-30M was made by adding 0.9 g (0.01 mol) of BD and 0.15% of additional catalyst to the reaction mixture of compound I and stirring at 75 °C for 2 h. The product was then precipitated with water and dried.

**c. ET-38M.** The polyether–polyurethane containing three MDI units extended with 1,4-butanediol (BD) was prepared as described by reaction Scheme II. A mixture consisting of 11 g (0.74 mol) of hexamethyldisilazane and 80 g (0.89 mol) of chlorotrimethylsilane was added to a solution of 200 g (2.2 mol) of 1,4-butanediol in 100 $cm^3$ of anhydrous ether. Rapid stirring was continued until precipitation of $NH_4Cl$ was complete. The solution was then fractionated by vacuum distillation and the desired 4-(trimethylsiloxyl)-1-butanol (compound II) was collected at

**Scheme II**

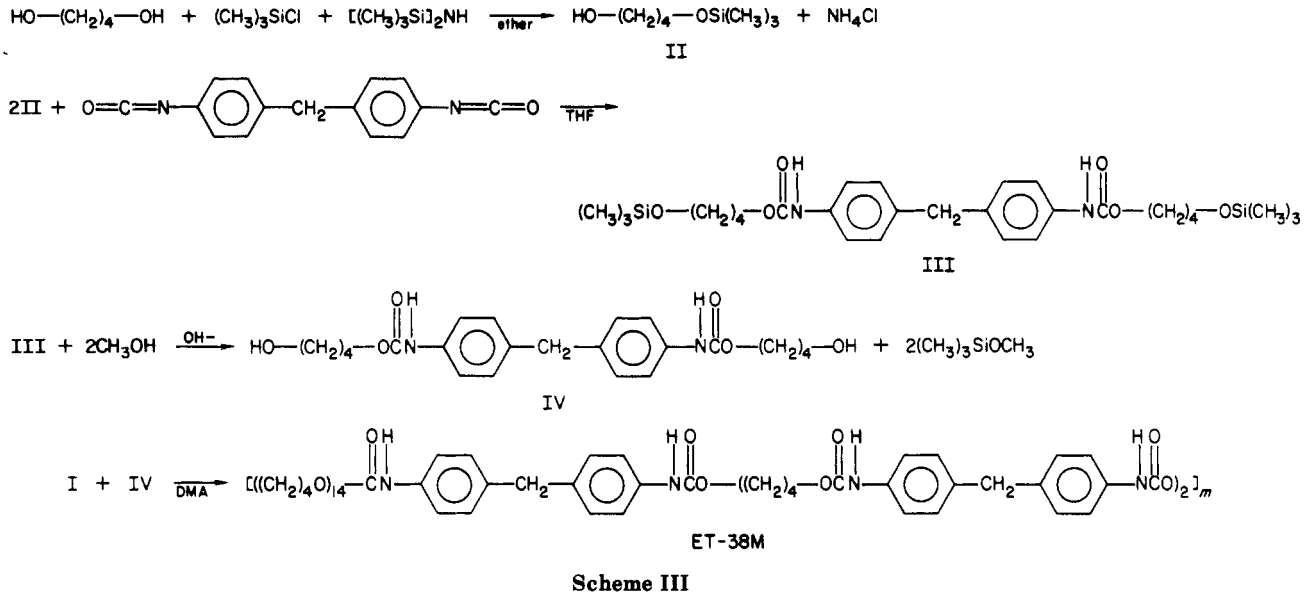

**Scheme III**

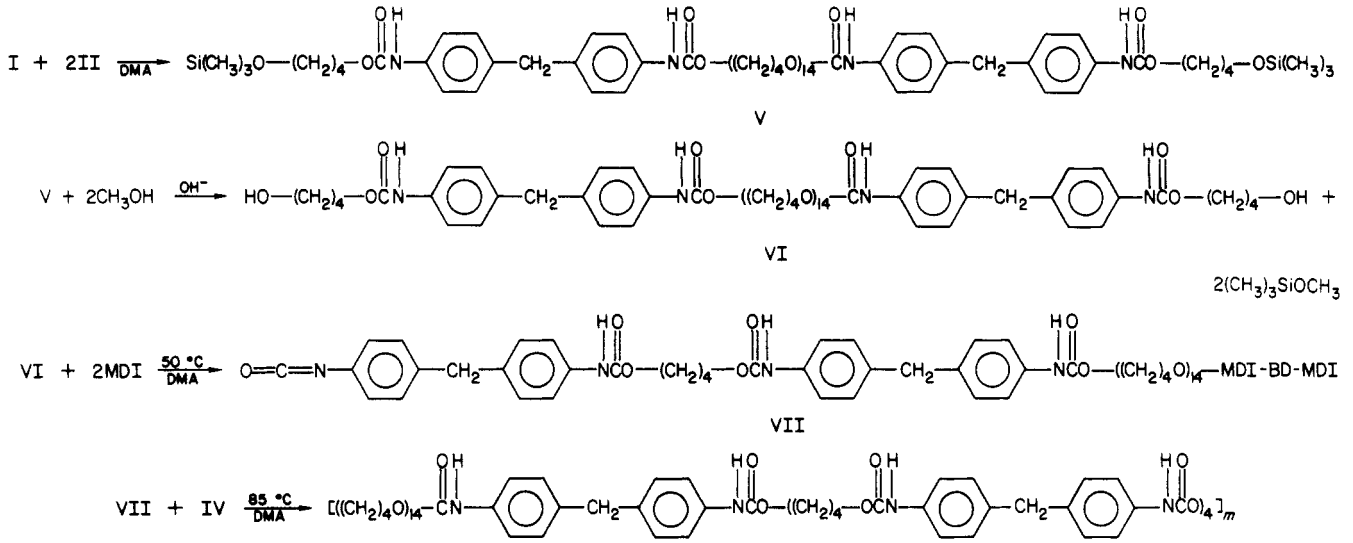

84–86 °C (4 mmHg). Compound II was then further purified by using a silica gel column eluted with the binary solvent of ether and pentane (9:1 v/v). The structure of compound II was confirmed by NMR spectroscopy (Figure 1). A mass spectrum of compound II (not shown) showed that a parent ion appeared at $m/e$ of 162 which was exactly the calculated molecular weight of compound II. Compound II was then linked with MDI to produce bis[(4-trimethylsiloxy)butyl] 4,4′-methylenebis(phenylcarbamate) (compound III). In order to accomplish this procedure, a solution of 25 g (0.1 mol) of MDI in 100 mL of dry THF was added over a period of 1 h to a solution of 40.5 g (0.25 mol) of compound II in 50 $cm^3$ of dry THF at 50 °C. A trace of catalyst (stannous octoate) was used. The process was completed after an additional hour of stirring. Because of the high reactivity of the isocyanate group with the hydroxyl group, this reaction was assumed to go to completion, although no characterization was done at this step.

To make compound IV, 500 mL of anhydrous methanol mixed with 150 $cm^3$ of dry dimethyl sulfoxide ($Me_2SO$) was added to replace the trimethylsilane groups of compound III with hydroxyl groups using potassium carbonate (2.4 mmol) as a catalyst. The reaction mixture was stirred at 0 °C for 1 h to complete the reaction. Acetic acid (24 mmol) was then added to neutralize the catalyst (potassium carbonate) at room temperature followed by adding distilled water to extract the precipitated inorganic salts. The resulting product (compound IV) was then washed and filtered with methanol/water (50:50 v/v).

To synthesize ET-38M, equimolar amounts of compound I and compound IV were mixed into DMA and allowed to react at 75 °C for 2 h with 0.15% of stannous octoate. The product was then precipitated and dried under vacuum.

**d. ET-48M.** The polyether–polyurethane containing five MDI units was synthesized by following reaction Scheme III. Compound II (4-(trimethylsiloxyl)-1-butanol) and compound I (MDI–PTMO–MDI) were mixed in a 2:1 molar ratio in DMA solution (30% w/v). After stirring for 2 h, a mixture of anhydrous methanol and $Me_2SO$ with the catalyst (potassium carbonate) was used as previously described to recover the hydroxyl group of compound V. This resulted in compound VI. Compound VII was made by capping compound VI with MDI using mild reaction conditions (50 °C and 30% w/v in DMA). As was the case for the capping reaction in Scheme I, the result of this capping step is not a pure species. The actual distribution will be described in the discussion of all of the distributions. Compound VII is therefore an average structure produced by this reaction. After stirring for 1 h, compound IV in DMA solution containing 0.15% of stannous octoate was added to the solution of compound VII solution in a 1:1 molar ratio. The mixture was stirred at 85 °C for 2 h. IR spectroscopy was used to verify the reaction completion. The final product was precipitated and dried in a vacuum.

**3. Synthesis of Materials by the Single-Step Method.** Polyether–polyurethanes produced by a random one-step method with the same stoichiometry as the ET-38M and ET-48M were prepared. MDI, BD, and PTMO were mixed in the appropriate molar ratios in DMA (30% w/v). Reactions were carried out at 80–90 °C for 3 h with 0.15% stannous octoate as catalyst.

**B. Determination of Hard Segment Length Distributions.** In order to properly compare the single-step (series S) polymers

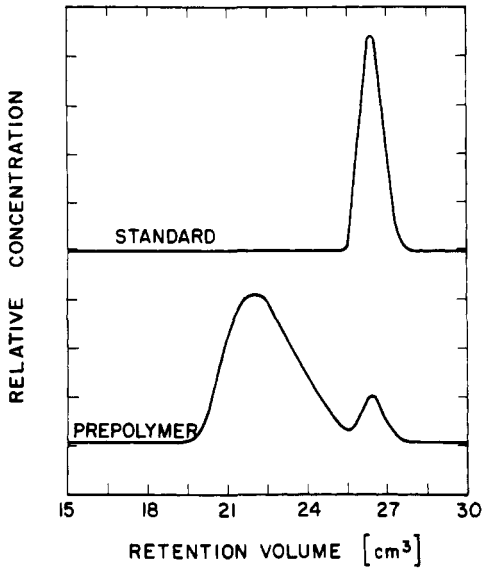


**Figure 2.** GPC chromatograms of prepolymer compound I and IPA–MDI–IPA standard.

with the multistep (series M) materials, it was necessary to determine how each of the reaction pathways affects the length distribution of the hard segments in the final polymer. Peebles[13,14] has done much of the theoretical work concerning the distribution of hard segment sizes in condensation block copolymers.

Calculation of the hard segment length distribution by the method of Peebles requires knowing the relative reactivity of the two isocyanate groups on the MDI for the system under investigation. As the ratio of these reactivities, $\mu$, gets larger, the intermediate products of a two-step reaction, and hence the hard segment length distribution, become more monodisperse. When $\mu = 1$, the size distribution for a two-step reaction is equivalent to that for a one-step reaction, i.e., the most probable distribution. Verstandig and Scherrer[15] reported a value of $\mu$ of 3.2 for the reaction of ethanol and MDI in toluene at 30 °C. Brock[16] obtained a value of $\mu$ of 2.9 for the reaction of butanol and MDI in toluene at 40 °C with triethylamine as a catalyst.

The reactivity ratio for the reaction of MDI and PTMO in DMA at 50 °C was determined by using gel permeation chromatography (GPC). A reference solution of MDI capped with isopropyl alcohol (IPA) was prepared by reacting a large excess of IPA with MDI and removing the excess IPA by vacuum drying. Twenty milligrams of this product, IPA–MDI–IPA, was dissolved in 20 cm$^3$ of THF, and a GPC chromatogram was obtained by using a Waters 501 ALC/GPC equipped with a refractive index detector. The columns used were a Shodex A-802 column and two Shodex A-80M columns, and the flow rate was 1 cm$^3$/min, with THF as the mobile phase.

To find the amount of excess MDI present after the first step of the reaction (2 MDI + 1 PTMO → products, 50 °C in DMA), the mixture of the products was reacted with a large excess of IPA. After vacuum drying to remove the DMA and excess IPA, the only species present are those terminated with IPA. A GPC chromatogram was run on this product mixture, and the results indicated that some free MDI was present in the initial product mixture. Free MDI corresponds to some linking of the polyol units by the MDI, and hence $\mu < \infty$. If $\mu$ is sufficiently large, there would be no free MDI and the "capping" reaction would be perfect, producing only MDI–PTMO–MDI. By comparing the peak area corresponding to IPA–MDI–IPA in the reference sample and the reaction sample, the percentage of the initial MDI used in the polyol–MDI capping reaction that persists as free MDI can be determined by knowing the total sample weight injected for the reference and reaction samples. This technique of using GPC on the first step oligomers in a two-step polyurethane elastomer reaction is more fully described by Bonart and Demmer.[17] The two chromatograms described above are shown in Figure 2.

The reactivity ratio $\mu$ can be calculated from the implicit equation of Peebles[13]

$$\mu(X_1^0/A_1)^{(1/2\mu)} + (\mu - 1)(X_1^0/A_1) = (2\mu - 1)(A_1 - B_1)/A_1 \quad (1)$$

where $X_1^0$ is the number of moles of free MDI present after the first stage of reaction, the capping step, $A_1$ is the initial number of moles of MDI used, and $B_1$ is the initial number of moles of PTMO used. The value of $\mu$ obtained from four trials of the capping reaction was 1.5 ± 0.2. Running the capping reaction at 50 and 90 °C yielded the same value of $\mu$. This implies that the activation energy for the reaction of each isocyanate group on MDI is the same.

After $\mu$ was determined, the dispersity of the hard segments in each polymer was calculated. For ET-20M, which is really a one step product but classified as a multistep becaues the hard segments are all one unit in length, $\bar{K}_w = \bar{K}_n = 1$ and $\bar{K}_w/\bar{K}_n = 1$, where $\bar{K}_w$ and $\bar{K}_n$ are the weight- and number-average values of MDI units per hard segment for complete conversion of monomer to polymer. ET-30S, a sample not prepared in this study, would have $\bar{K}_w = 3.0$ and $\bar{K}_n = 2.0$ for a polydispersity index $\bar{K}_w/\bar{K}_n$ of 1.5.[14] The dispersity for ET-30M can be found by using the equations given by Peebles.[14]

$$\bar{K}_n = A_1/B_1 \quad (2a)$$

$$\bar{K}_w = \left[A_1 + C_1 + C_1\left(\frac{1+p}{1-p}\right)\right] \Big/ A_1 \quad (2b)$$

In this equation $C_1$ is the number of moles of chain extender used, in this case butanediol, and $p$ is defined by

$$p = X_1^0/C_1 \quad (3)$$

For ET-30M, $X_1^0$ was calculated to be 0.423 on the basis of GPC results, so $\bar{K}_w = 2.74$ and $\bar{K}_n = 2.00$, yielding a polydispersity index of 1.37.

For the sample ET-38S, eq 2a and 2b yield $\bar{K}_w = 5.00$ and $\bar{K}_n = 3.00$, so $\bar{K}_w/\bar{K}_n = 1.67$. The polydispersity of the sample ET-38M is harder to obtain, as in this case the chain extender is not butanediol but rather compound IV, bis(4-hydroxybutyl) 4,4′-methylenebis(phenylcarbamate), abbreviated BMB. This chain extender contains an MDI unit which must be included in the distribution calculations.

From the definition of number and weight averages one can derive[14]

$$\bar{K}_n = \frac{X_1^0 + \sum_{i=1}^{\infty}(i+1)P_i}{X_1^0 + \sum_{i=1}^{\infty}P_i} \quad (4a)$$

and

$$\bar{K}_w = \frac{X_1^0 + \sum_{i=1}^{\infty}(i+1)^2P_i}{X_1^0 + \sum_{i=1}^{\infty}(i+1)P_i} \quad (4b)$$

where $P_i$ is the number of hard segment sequences that contain $(i + 1)$ MDI units, or alternatively, $i$ chain extender units. This is strictly for the case where the chain extender does not contain an MDI unit. For the case where the chain extender contains an MDI unit, the same $P_i$ values can be used, but the number of MDI units per hard segment must be modified to $2i + 1$. Now

$$\bar{K}_n = \frac{X_1^0 + \sum_{i=1}^{\infty}(2i+1)P_i}{X_1^0 + \sum_{i=1}^{\infty}P_i} \quad (5a)$$

and

$$\bar{K}_w = \frac{X_1^0 + \sum_{i=1}^{\infty}(2i+1)^2P_i}{X_1^0 + \sum_{i=1}^{\infty}(2i+1)P_i} \quad (5b)$$

To calculate the dispersity of ET-38M, we start with the results for ET-30M to find the numeric values for the summations of the $P_i$'s, as the values of $P_i$ are the same for both ET-30M and

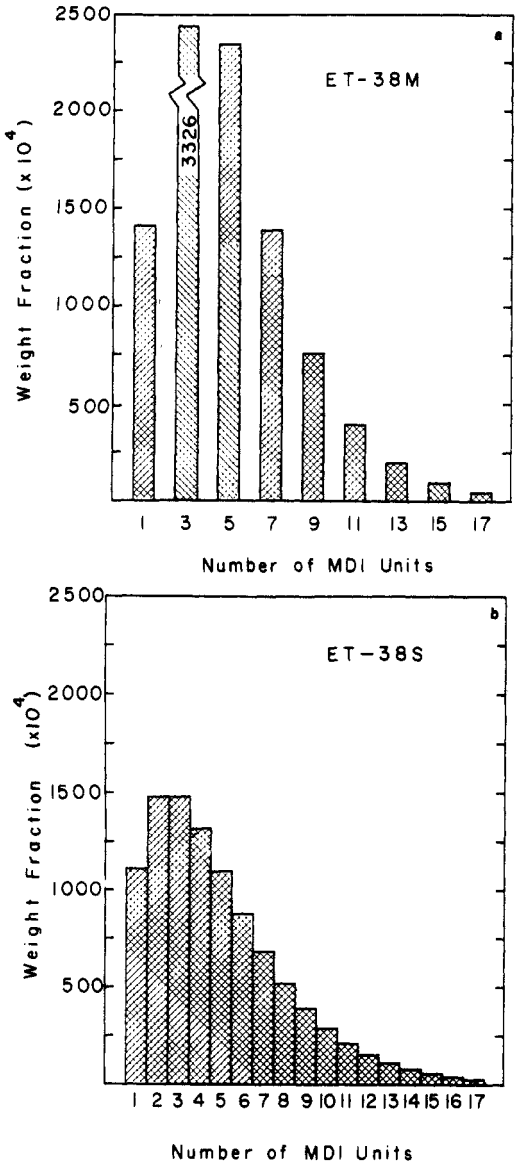


**Figure 3.** (a) Histogram of ET-38M weight fraction distributions. (b) Histogram of ET-38S weight fraction distributions.

ET-38M when ET-38M is made using BMB as a chain extender. Starting with a material balance, with $A_1 = 2$, $B_1 = C_1 = 1$, and $\mu = 1.5$, we get

$$X_1^0 + \sum_{i=1}^{\infty} P_i = 1 \tag{6a}$$

$$X_1^0 + \sum_{i=1}^{\infty} (i+1)P_i = 2 \tag{6b}$$

$$X_1^0 + \sum_{i=1}^{\infty} (i+1)^2 P_i = 5.47 \tag{6c}$$

Expanding eq 5b and substituting in eq 6a–c one obtains the result $\bar{K}_w = 4.96$ and $\bar{K}_w/\bar{K}_n = 1.65$. Thus the dispersity of ET-38M is approximately the same as that for ET-38S. However, the exact distributions are different, as will be discussed.

The distribution of sequence lengths in the ET-38 materials is assumed to follow most probable statistics, after Peebles.[13,14] We start by calculating the distribution for the one-step material. Equation 1 is solved by using $\mu = 1$, $A_1 = 3$, and $B_1 = 1$. Setting $\mu = 1$ for a multistep reaction yields the statistics for a single-step reaction.[13] The solution to eq 1 for these parameter values yields $X_1^0 = 1.333$. The number of internal MDI units, $X_1^{int}$, which is the number of hard segment units containing one MDI, is given by[13]

$$X_1^{int} = 2B_1 + X_1^0 - A_1 \tag{7}$$

**Table II**
**Hard Segment Distributions for the ET-38 Polymers**

| | mol fraction × $10^4$ | | wt fraction × $10^4$ | |
|---|---|---|---|---|
| no. of MDI's | multistep | single step | multistep | single step |
| 1 | 4233 | 3333 | 1411 | 1111 |
| 2 | 0 | 2222 | 0 | 1481 |
| 3 | 3326 | 1481 | 3326 | 1481 |
| 4 | 0 | 988 | 0 | 1317 |
| 5 | 1408 | 658 | 2346 | 1097 |
| 6 | 0 | 439 | 0 | 878 |
| 7 | 596 | 293 | 1391 | 683 |
| 8 | 0 | 195 | 0 | 520 |
| 9 | 252 | 130 | 757 | 390 |
| 10 | 0 | 87 | 0 | 289 |
| 11 | 107 | 58 | 392 | 212 |
| 12 | 0 | 39 | 0 | 154 |
| 13 | 45 | 26 | 196 | 111 |
| 14 | 0 | 17 | 0 | 80 |
| 15 | 19 | 11 | 96 | 57 |
| 16 | 0 | 7.6 | 0 | 41 |
| 17 | 8.1 | 5.1 | 46 | 29 |
| 18 | 0 | 3.4 | 0 | 20 |
| 19 | 3.4 | 2.2 | 22 | 14 |
| 20 | 0 | 1.5 | 0 | 10 |

**Table III**
**Hard Segment Distributions for the ET-48 Polymers**

| | mol fraction × $10^4$ | | wt fraction × $10^4$ | |
|---|---|---|---|---|
| no. of MDI's | multistep | single step | multistep | single step |
| 1 | 4233 | 2000 | 847 | 400 |
| 2 | 0 | 1600 | 0 | 640 |
| 3 | 1499 | 1280 | 899 | 768 |
| 4 | 0 | 1024 | 0 | 819 |
| 5 | 1280 | 819 | 1280 | 819 |
| 6 | 0 | 655 | 0 | 786 |
| 7 | 896 | 524 | 1254 | 734 |
| 8 | 0 | 419 | 0 | 671 |
| 9 | 627 | 336 | 1129 | 604 |
| 10 | 0 | 268 | 0 | 537 |
| 11 | 439 | 215 | 966 | 472 |
| 12 | 0 | 172 | 0 | 412 |
| 13 | 307 | 137 | 799 | 357 |
| 14 | 0 | 110 | 0 | 308 |
| 15 | 215 | 88 | 645 | 264 |
| 16 | 0 | 70 | 0 | 225 |
| 17 | 151 | 56 | 512 | 191 |
| 18 | 0 | 45 | 0 | 162 |
| 19 | 105 | 36 | 400 | 137 |
| 20 | 0 | 29 | 0 | 115 |
| 21 | 74 | 23 | 310 | 97 |
| 22 | 0 | 18 | 0 | 81 |
| 23 | 52 | 15 | 238 | 68 |
| 24 | 0 | 12 | 0 | 57 |
| 25 | 36 | 9 | 181 | 47 |

For the one-step 3/2/1 case $X_1^{int} = 0.333$. The distribution follows the form

$$N_i = N_1 p^{i-1}$$

where $N_i$ is the number of chain extenders per hard segment. A mole balance on the total hard segments and on the total number of chain extenders yields $N_1$ and $p$. Similarly, the distribution for the multistep reaction can be found. The results of the distributions are summarized in Table II, with the weight fraction distributions for the ET-38 materials shown in Figure 3a,b. The most interesting features are that the multistep reaction contains substantially more hard segments with one MDI unit, a phenomenon that promotes phase mixing, and that the multistep reaction has no even numbers in the hard segment length distribution.

By a similar procedure, the distributions and averages for the 5/4/1 materials can be calculated. For the one-step sample, $\bar{K}_w = 9.00$ and $\bar{K}_w/\bar{K}_n = 1.80$. This is a correction to the value in Table I reported by Peebles.[14] For the multistep synthesis, $\bar{K}_w$

= 10.60 and $\bar{K}_w/\bar{K}_n$ = 2.12. The distributions for these samples are summarized in Table III.

**C. Preparation of Samples.** Films of the polyurethanes were spin cast from a solvent mixture of THF and DMA in a 3:1 volume ratio, dried in a vacuum oven at 55 °C for 1 week, and then stored in a desiccator at room temperature.

**D. Testing of Samples. 1. Fourier Transform Infrared Spectroscopy.** Infrared absorbance spectra of thin films were obtained by using a Nicolet 7199 Fourier transform infrared spectrophotometer under dry air purge. One hundred scans at a resolution of 2 $cm^{-1}$ were signal averaged before Fourier transformation. The IR absorbance of C=O region was resolved into free and hydrogen-bonded peaks by using a computer program to fit peaks as combined Gaussian or Lorentzian curves via nonlinear least-squares regression.

**2. Differential Scanning Calorimetry.** DSC thermograms over the temperature range from −120 to about 250 °C were recorded on a Perkin-Elmer DSC-II interfaced with a thermal analysis data station. Calibration was done by using indium and mercury as standards. The experiments were carried out at a heating rate of 20 °C/min under helium purge on samples weighing 16 ± 2 mg. A scanning auto zero module was used to minimize instrumental nonlinearity over the temperature range of interest.

The annealing experiments were carried out in situ in the DSC apparatus. Samples were heated from −90 to +230 °C to obtain the control DSC trace and then quenched to 130 °C and held for 5 h for all M-series and S-series materials except ET-20M, whose corresponding hard segment model compound, $CH_3CH_2O$–MDI–$OCH_2CH_3$, exhibited a melting temperature of 129 °C.[21] ET-20M was annealed at 70 °C. No melting or crystallization was observed during the preheating procedure (−90 → 230 → 130 or 70 °C) or in any of the control samples.

**3. Dynamic Mechanical Analysis.** Dynamic mechanical data were collected at 110 Hz by using a Toyo Rheovibron DDV-IIC apparatus which was controlled automatically by a computer. Film samples, about 0.04 × 3 × 20 mm in size, were tested under a nitrogen blanket from −150 to 200 °C at a heating rate of 2 °C/min.

**4. Tensile Testing.** Uniaxial stress–strain measurements at room temperature were made by using an Instron tensile testing machine with a crosshead speed of 0.5 in./min. Dumbbell-shaped film samples with a gauge length of 1.5 in. were stamped out with an ASTM 412 die. The engineering stress was calculated as the force divided by the initial cross-sectional area. Reported data are the average of three tests.

Tensile hysteresis measurements were made by loading and unloading the specimen at a crosshead speed of 0.5 in./min. These experiments were carried out to increasing strain levels. The percent hysteresis for a given cycle was calculated from the ratio of the area bounded by the loading–unloading curves to the total area under the loading curve. Permanent set was arbitrarily recorded as the percent strain where the stress dropped to zero on the reverse strain cycle in the hysteresis test.

**5. Wide-Angle X-ray Diffraction.** Wide-angle X-ray diffraction (WAXD) experiments were performed by using a Picker Model 3677A diffractometer. The X-ray beam was nickel-filtered Cu K$\alpha$ ($\lambda$ = 0.1542 nm) radiation from a sealed tube operated at 35 kV and 15 mA. Data were obtained from 6° to 35° (2$\theta$) at a scan rate of 1°/min with a smoothing time constant of 3 s.

**6. Small-Angle X-ray Scattering.** X-rays were produced by a rotating-anode X-ray generator operated at a 40-kV accelerating potential and a 50-mA emission current. A nickel filter was used to select Cu K$\alpha$ X-rays as the primary wavelength. A modified Kratky compact SAXS camera was used to collimate the X-rays into a beam which was about 1.25 cm by 100 $\mu$m at the sample. The collimation optics, the sample holder, and the enclosed scattering path were evacuated to minimize scattering by air. The sample-to-detector distance was approximately 0.6 m. Scattered X-rays were detected by a one-dimensional position-sensitive detector and associated electronics. The SAXS data were collected by a multichannel analyzer and transferred to a computer for subsequent processing. Corrections were made to the data to take into account the detector sensitivity, the detector dark current, parasitic scattering, and sample absorption. Relative intensity data were converted to absolute intensity data by using a Lupolen (polyethylene) standard.[31] In order to eliminate slit-length smearing effects, an experimentally measured slit-length weighting function was used to desmear the data by the iterative method of Lake.[32] The range of sample thicknesses was from about 0.2 to 0.5 mm, and the range of linear attenuation coefficients varied from about 0.6 to 0.7 $mm^{-1}$.

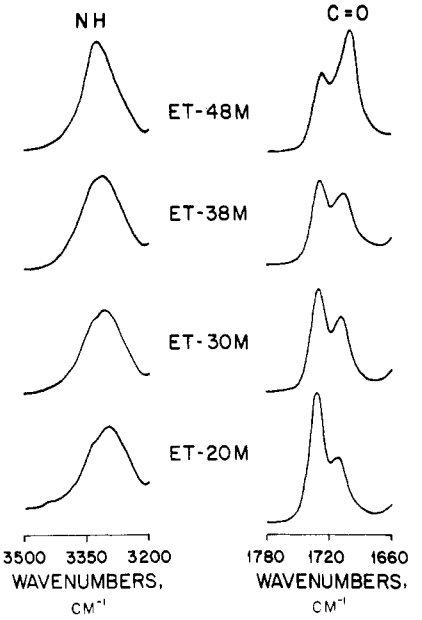


**Figure 4.** Infrared spectra of the multistep polyurethanes in the NH and C=O stretching regions.

## III. Results and Discussion

**A. Infrared Spectroscopy.** FTIR spectroscopy was used to investigate the degree of hard and soft segment interaction in these samples. In a pure urethane hard domain, hydrogen bonding results from the hydrogen atoms of NH groups serving as proton donors and the C=O groups acting as proton acceptors. When the urethane hard segment and the PTMO soft segment are mixed at the molecular level, the oxygens in the PTMO backbone also act as proton acceptors in forming hydrogen bonds with the NH groups of the hard segment urethane groups.

Figure 4 shows the IR spectrum for each multistep material in the NH and C=O stretching absorption regions. The NH absorption region (located between 3500 and 3200 $cm^{-1}$) indicates nearly complete hydrogen bonding for each sample. The free NH stretching band near 3420 $cm^{-1}$ was not observed. The bonded NH absorption peak shown in Figure 4 shifts to slightly higher wavenumbers (higher energy) as the hard segment content increases. Quantitative analysis of this observation was not attempted. In the carbonyl absorption region between 1780 and 1660 $cm^{-1}$, the carbonyl absorption band splits into two peaks. The peak due to bonded C=O stretching is centered at 1700 $cm^{-1}$ and that due to free C=O stretching is centered at 1732 $cm^{-1}$. It is clearly seen that the fraction of bonded C=O absorbance increases as the hard segment length is increased (from ET-20M to ET-48M). The interurethane bonded hard segments (NH···O=C) are generally regarded as residing in the interior of the hard domains, while the hard segments possessing free C=O groups are present in the mixed soft phase or at the interface.[18] Since it is known that the extinction coefficients of free C=O and bonded C=O are about the same,[19,20] the fraction of hard segments participating in urethane–urethane hydrogen bonding is given by

$$X = \frac{A_{C=O,b}}{A_{C=O,b} + A_{C=O,f}} \quad (8)$$

**Table IV**
**FTIR Results Based on Carbonyl Absorption Peaks**

| sample | hard segment wt fraction[a] | fraction of interurethane bonded C=O's[b] | wt fraction of hard segments dissolved in soft domains[c] |
|---|---|---|---|
| ET-20M | 0.23 | 0.37 | 0.15 |
| ET-30M | 0.39 | 0.51 | 0.24 |
| ET-38M | 0.50 | 0.50 | 0.33 |
| ET-48M | 0.63 | 0.70 | 0.34 |
| ET-38S | 0.50 | 0.74 | 0.21 |
| ET-38SA[d] | 0.50 | 0.78 | 0.18 |
| ET-48S | 0.63 | 0.79 | 0.26 |
| ET-48SA[d] | 0.63 | 0.80 | 0.25 |

[a] See Table I for calculation of hard segment weight fraction, $W(HS)$. [b] Fraction of interurethane bonded C=O's, $x$, was calculated by using eq 8 in text. [c] The weight fraction of hard segments dissolved in soft domains, $W(HS/SD)$, was calculated by using the relation $W(HS/SD) = [1 - x]W(HS)/[[1 - x]W(HS) + [1 - W(HS)]$. This calculation assumes that there are no soft segments dissolved in hard domains and that all noninterurethane bonded C=O's are located in the soft domains. [d] Samples designated SA were annealed for 5 h at 130 °C.

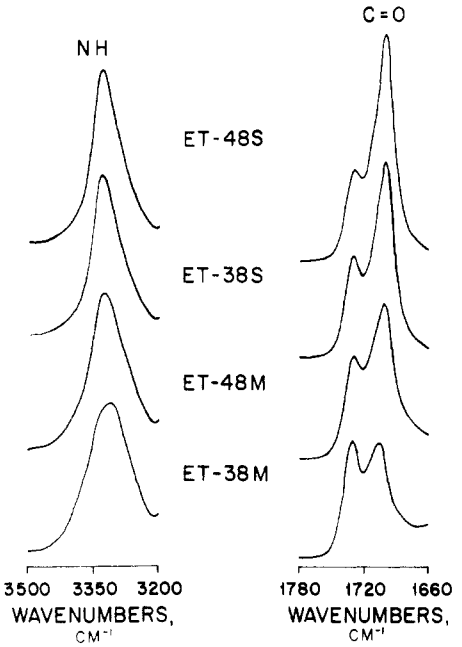


**Figure 5.** Infrared spectra of ET-38M, ET-38S, ET-48M, and ET-48S in the NH and C=O stretching regions.

where $A_{C=O,b}$ is the area of the bonded carbonyl absorption and $A_{C=O,f}$ is the area of the free carbonyl absorption.

Table IV shows the FTIR results calculated by using the free and bonded carbonyl peak areas. If one assumes that there are no soft segments dissolved in the hard domain and that all carbonyls in the hard domain are bonded, then $X$ is just the fraction of hard segments located in the interior of the hard domains. If the assumption is made that each material consists of soft and hard phases, then $X$ is a lower bound on the weight fraction of hard domains. With the same assumptions, the values given in Table IV for the weight fraction of hard segments in soft domains are upper bounds.

The FTIR results for the multistep materials, which are consistent with previous results,[8] show that an increase in hard segment content leads to a higher hard domain content as well as a higher fraction of hard segments dissolved in the soft domains.

Figure 5 shows a comparison of FTIR spectra of the single-step and multistep samples. The results given in Table IV indicate that the multistep materials are more

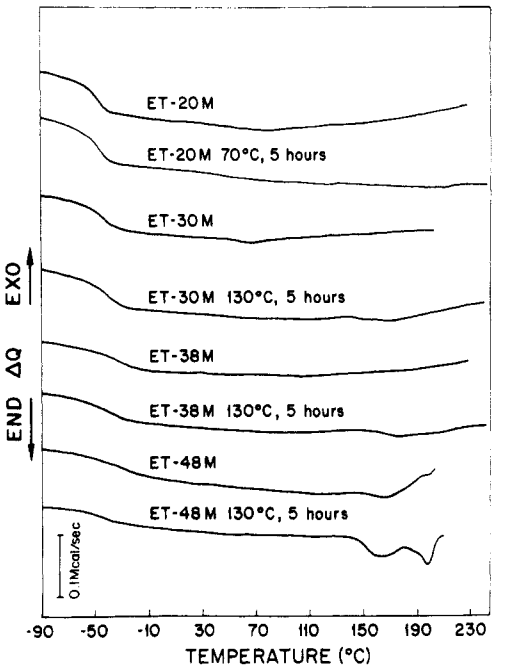


**Figure 6.** DSC curves of the multistep polyurethanes; annealing temperatures indicated.

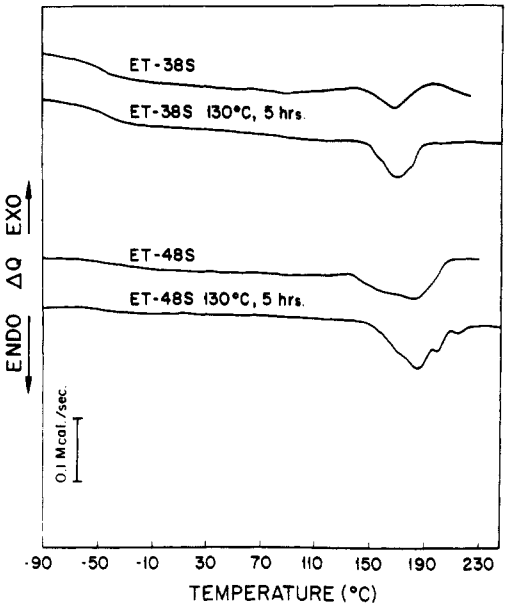


**Figure 7.** DSC curves of randomly polymerized polyurethanes; annealing histories indicated.

phase mixed than the single-step materials. The increased phase mixing is attributed to the higher fraction of single MDI unit hard segments in the multistep materials. That is, the presence of more soluble, short hard segments promotes phase mixing. The results also indicate that annealing causes a slight increase in phase separation, i.e., more hard segments in hard domains and fewer in soft domains.

**B. Differential Scanning Calorimetry (DSC).** The results of DSC studies on the multistep samples and their single-step analogues for both control and annealed samples are shown in Figures 6 and 7 and are summarized in Table V.

Figure 6 shows the DSC results of the M-series materials. ET-20M, in which the hard segments contain only one MDI unit, displayed essentially identical DSC traces before and after annealing at 70 °C. The glass transition temperature remained constant at −49 °C, indicating no de-

Table V
DSC and Dynamic Mechanical Test Results

| material | thermal history | $T_g$, °C (DSC) | $T_g$, °C ($E''$ peak) | melting endotherm(s), °C |
|---|---|---|---|---|
| ET-20M | control | -49 | -44 | |
| | 70 °C, 5 h | -49 | | |
| ET-30M | control | -44 | -42 | |
| | 130 °C, 5 h | -43 | | |
| ET-38M | control | -41 | -37 | |
| | 130 °C, 5 h | -40 | | 173 |
| ET-48M | control | -29 | -25 | 170 |
| | 130 °C, 5 h | -46 | | 165, 199 |
| ET-38S | control | -46 | -39 | 167 |
| | 130 °C, 5 h | -49 | | 167 |
| ET-48S | control | -42 | -21 | 185 |
| | 130 °C, 5 h | -50 | | 182, 197, 212 |

tectable annealing-induced phase separation. This is in contrast to Kwei's[22] finding that annealing at a temperature lower than 80 °C (for periods as short as 1 h) improved the phase separation in a PTMO-based polyurethane containing 22.0% MDI. Kwei argued that annealing below 80 °C excluded both short and long hard segments from the soft phase while annealing at a temperature higher than 80 °C excluded only the long hard segments from the soft segment phase. As shown in the previous study on blends of PTMO and monodisperse urethane model compounds,[21] a hard segment with one MDI unit blended with PTMO can crystallize into a phase with a melting temperature of 50 °C. Also, in piperazine-based polyurethanes the hard segment which has a molecular weight equivalent to that of one MDI unit readily crystallizes.[9,10] There appear to be two factors which inhibit the crystallization of hard segments containing MDI units. The first is the constraint on hard segment mobility caused by the covalent joints between the hard and soft segments, and the second is hard segment–soft segment hydrogen bonding. According to IR analysis of ET-20M (Table IV), only 37% of the urethane NH groups form interurethane hydrogen bonds, so a substantial fraction of hydrogen bonding to the ether groups of PTMO is present.

Similar to ET-20M, the DSC traces of the control samples of ET-30M and ET-38M show no melting and only a glass transition at -44 and -41 °C, respectively. However, after annealing at 130 °C, ET-30M shows a barely detectable, diffuse endotherm in the range 147–167 °C, while ET-38M shows a diffuse melting endotherm at 173 °C. Both of these events occur at far lower temperatures than in a blend of PTMO (1000 MW) and a 3/2 MDI/BD monodisperse model hard segment terminated on both ends with ethanol, where the melting endotherm was at 232 °C.[23] The ET-48M sample shows a melting endotherm at 170 °C, indicative of hard segment crystallinity. After annealing at 130 °C the ET-48M soft segment $T_g$ dropped from -29 °C to -46 °C, which suggests that annealing improved the phase separation. Annealing of ET-48M at 130 °C also caused two well-defined endotherms (at 165 and 199 °C) to appear. The appearance of two endotherms rather than one can be explained either by the presence of crystalline lamellae with different thicknesses or by the presence of hard segment crystallites with different crystal structures (polymorphism).

Figure 7 shows the DSC thermograms of the materials made by the single-step process. A broad melting endotherm at 167 °C was observed for the ET-38S control sample. Annealing at 130 °C enhanced this endotherm without shifting the melting point. Annealing also slightly decreased $T_g$. An almost identical result was found by Van Bogart et al.[25] in their DSC measurements on a similar

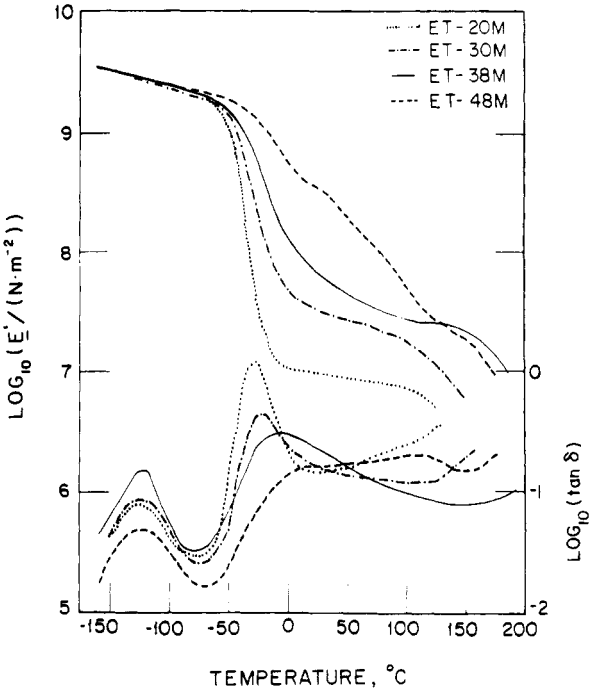


Figure 8. Dynamic mechanical properties of the multistep polyurethanes.

sample (ET-38-bulk polymerized) which was annealed at 120 °C for 4 days. Earlier, Hesketh et al.[24,26] studied a series of polyurethanes which were annealed at various temperatures between 120 and 190 °C. They reported that the fraction of hard segments dissolved in the soft phase increased with increasing annealing temperature, based on the elevation of the soft segment $T_g$. It should be noted that the critical length below which the hard segments dissolve in the soft segment phase increases with increasing temperature.

Compared with the DSC results of ET-38M, ET-38S shows a lower soft segment $T_g$ (Table V) and a much more distinct high temperature melting endotherm upon heating. This is consistent with the results of IR analysis, suggesting that better phase separation occurs in the ET-38S sample. This is because the single MDI hard segments are more soluble in the soft phase than the longer units, and ET-38S has fewer single units than does ET-38M. On the basis of the DSC results, it appears that the hard segments containing more than three MDI units which exist in the ET-38S material serve more effectively as crystal nucleation sites. The hard segments accumulate laterally if their lengths are long enough to form a stable crystal phase at the corresponding annealing temperature. The annealing of ET-48S gives more complex thermograms than are produced by annealing of ET-38S. ET-48SA, when annealed at 130 °C, shows multiple melting endotherms with peak temperatures at 182, 197, and 212 °C. The soft segment glass transition appears at about -50 °C for ET-48SA and the heat of fusion calculated from the endotherm area was 7.55 cal/g.

**C. Dynamic Mechanical Analysis.** Figure 8 shows the dynamic mechanical response of the M-series of samples, while Figure 9 shows the effects of different hard segment size distributions on the dynamic mechanical spectra of the ET-38 and ET-48 systems. Table V lists the peak temperature of the $\beta$ relaxation in the $E''$ curve which is the polyether phase glass transition temperature measured in this test.

Figure 8 shows that as the hard segment concentration increases from ET-20M to ET-48M, a broadening in the

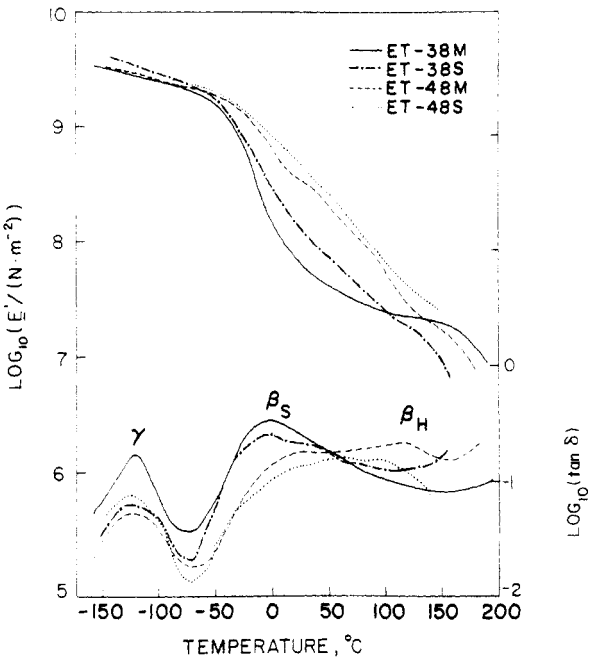


**Figure 9.** Dynamic mechanical properties of multistep and single-step ET-38 and ET-48 materials.

**Table VI**
**Tensile Properties**

| material | Young's modulus, MPa | stress at break, MPa | elongation at break, % |
|---|---|---|---|
| ET-20M | 3 | 7 | 1620 |
| ET-38M | 24 | 40 | 730 |
| ET-48M | 94 | 58 | 600 |
| ET-38S | 33 | 18 | 510 |
| ET-38SA | 41 | 25 | 450 |
| ET-48S | 136 | 30 | 360 |
| ET-48SA | 179 | 44 | 330 |

$\beta$ peak and an enhancement of the rubbery modulus is observed. This is due to an increase in the size and interconnectivity of the hard segment domains as the sample composition changes from a predominantly soft segment material to a predominantly hard segment material. The shift of the $\beta$ peak to higher temperature with increasing hard segment length can be attributed to a greater fraction of hard segments dissolved in the soft phase. The decrease in the magnitude of the $\beta$ peak with increasing hard segment length results from a decrease in the soft segment content.

Figure 9 shows the dynamic mechanical spectra for samples of ET-38 and ET-48. The polyurethanes made by the single-step process display a higher rubbery modulus and lower $\beta$ peak than their multistep analogues. This is due to a higher degree of phase separation which exists in samples of the S-series due to the lower fraction of single MDI hard segments, as indicated by IR and DSC results. Earlier studies by Ng et al.[9] on piperazine-based polyurethanes showed that hard segment polydispersity had no effect on the $\beta$ relaxation, but that a narrower distribution of hard segments resulted in a higher rubbery modulus. Ng et al. concluded that in the piperazine-based polyurethane system, phase separation was high regardless of the uniformity in hard segment length.

**D. Stress–Strain Analysis.** The stress–strain curves of the samples made by the two different pathways are shown in Figure 10, and the results are summarized in Table VI. The tensile behavior of a strained thermoplastic elastomer generally depends on the size, shape, and concentration of the hard domains, intermolecular bonding within the hard domains, and the ability of the soft segments to crystallize under strain. Among the polymers studied, only ET-20M possesses a stress–strain curve resembling a lightly cross-linked rubber above its $T_g$. The other materials tested exhibit the high toughness and strength typical of segmented polyurethanes. The substantial increase in modulus with increasing hard segment content is attributed to an increasing degree of interconnectivity of hard domains as the material changes from a predominantly soft segment one to a predominantly hard segment one.

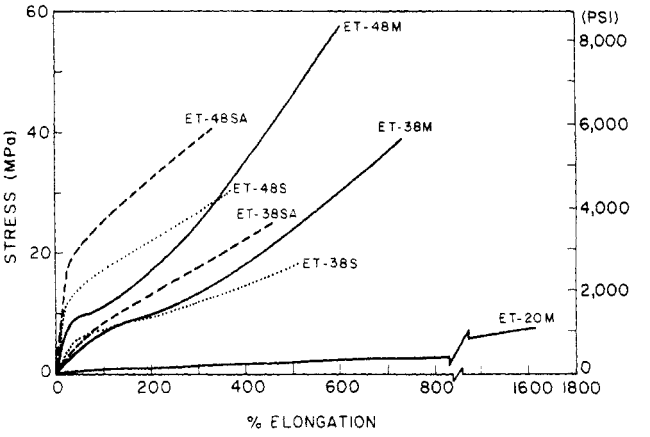


**Figure 10.** Stress–strain curves of the multistep polyurethanes and their single-step analogues.

The S-series materials, which contain fewer single MDI hard segments, exhibit a higher Young's modulus and lower ultimate strength and elongation at break when compared to corresponding multistep materials. The high Young's modulus of the S-series materials is consistent with the higher rubbery modulus observed in the dynamic mechanical test. Generally, two factors can enhance the toughness and plastic character of a two-phase polyurethane elastomer: the interconnectivity and the crystallinity of the hard segment domains. Both IR and DSC results show that the S-series possess better phase separation than the M-series materials so that the hard domain weight fraction is higher in S-series materials. DSC also shows the presence of crystalline domains in the S-series material, which may also explain why the S-series materials possess a higher Young's modulus than the M-series materials.

The enhancement of strength at large elongation in PTMO-based polyurethanes is often ascribed to strain-induced crystallization of the PTMO chains. While the M-series materials appear to strain harden, no significant strain hardening occurs in the S-series materials. The soft segments in the S-series polyurethanes may have more constraints imposed due to their hard segment domains which have a higher degree of hard segment crystallinity and are more interconnected. Annealing the S-series materals at 130 °C caused an improvement in tensile properties due to an increase in hard segment crystallinity within the hard domains.

Trends similar to the present study were found in the tensile property study of piperazine based polyurethanes.[10] Harrell reported that a narrower distribution of either the hard segment or the soft segment increased both the modulus and the tensile properties of the polyurethanes. However, the hard segment length distribution had a more significant effect than the soft segment length distribution. In the present study, the distribution of hard segment lengths in MDI/BD-based polyurethanes was found to affect the stress and elongation at break as well as Young's modulus.

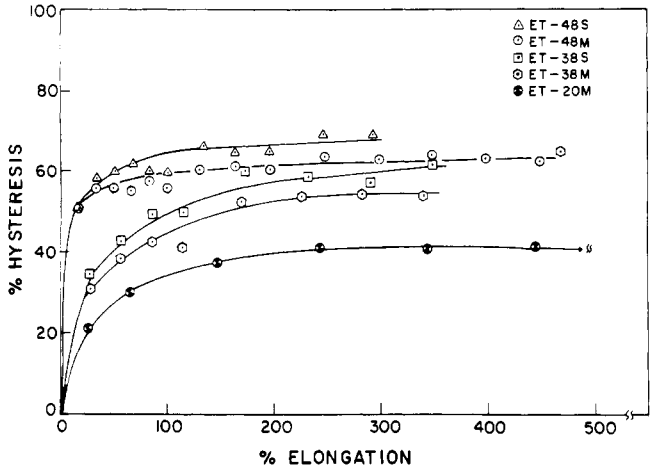


**Figure 11.** Hysteresis as a function of elongation for the multistep polyurethanes and their single-step analogues.

Figure 11 shows the hysteresis behavior for the M-series and S-series polyurethanes. In a multiphase material the hysteresis behavior is related to the morphology and the composition of the phases.[18,27,28] A high initial hysteresis can result from plastic deformation of a semicrystalline or glassy domain within the material or disruption of an interconnected hard domain morphology. For sample ET-48M, the hysteresis quickly reaches about 55% and ultimately reaches the a value of slightly more than 60% at 500% strain. This is typical hysteresis behavior for polyurethanes which possess interconnected hard domains.[2] The high hysteresis at low strains suggests very early plastic deformation of the semicrystalline hard domains. For sample ET-38M, the hysteresis reaches 30% at 25% elongation and then increases slowly with strain to 60% at an elongation of 500%. The hard segment domains in ET-38M are apparently interlocked, but with less interconnectivity than in ET-48M. Finally, ET-20M exhibits an initial hysteresis value of 20% at 25% elongation which increases slowly to 40% at 500% elongation. The hysteresis of ET-20M is lower than that of a 2,4-TDI/ethylenediamine/PTMO-2000 sample which had an isolated hard segmnt domain morphology according to Paik-Sung.[28]

The polymers made by the single-step process exhibit a higher hysteresis than the corresponding multistep samples over the entire strain range. This can be interpreted by the higher hard segment domain content and crystallinity of the S-series materials which increases their plastic deformation upon strain. This is further evidence of the significance of single MDI unit hard segments on the physical properties. A higher hard domain interconnectivity for S-series than for M-series materials may be proposed, although there is no significant difference in the initial hysteresis in both systems. It should also be pointed out that no change in the extent of interurethane hydrogen bonding occured upon straining the samples. This is consistent with some earlier studies on polyurethanes,[18] but other research has shown hydrogen bonding decreasing with deformation.[29] For the M-series and S-series materials, hysteresis is due to plastic deformation of the hard segment domains. Hydrogen bond disruption may occur, but in the strained state the hydrogen bonds rapidly reform, certainly within the time scale of the infrared experiment.

Figure 12 shows the permanent set vs. strain curves for both M- and S-series materials. Generally, rubbery materials possess a very low permanent set. In a multiphase block copolymer, an increase in the hard segment domain

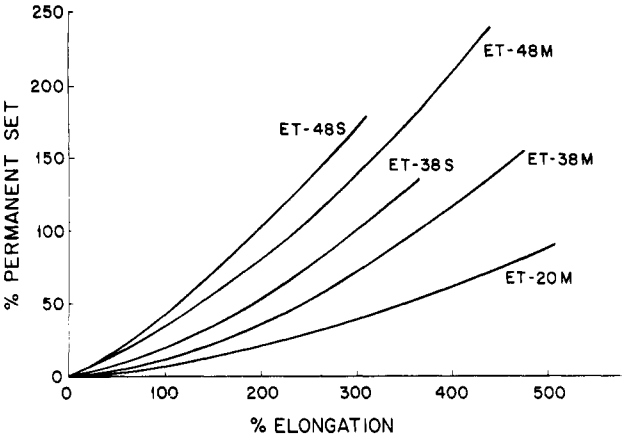


**Figure 12.** Extension set properties of the multistep polyurethanes and their single-step analogues.

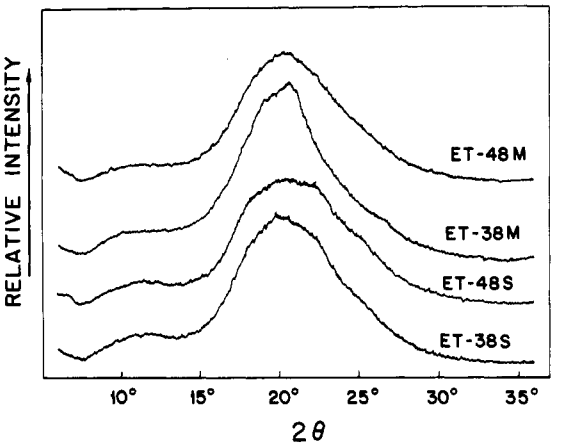


**Figure 13.** WAXD curves for ET-38M, ET-38S, ET-48M, and ET-48S.

interconnectivity causes an increase in the plasticity of the material and in the amount of permanent set. In the present study ET-20M has the lowest set, while ET-38M and ET-48M samples exhibit higher extension set due to their higher hard domain interconnectivity.

Figure 12 also shows that the polyurethanes made by the single step polymerization display a higher permanent set than their multistep counterparts. This can be attributed to higher hard domain interconnectivity in the S-series materials and to the fewer number of single MDI unit hard segments. In addition, the higher crystallinity of the S-series materials results in a higher plasticity, and thus a lower sample recoverability.

Harrell[10] reported that piperazine-based polyurethanes with monodisperse hard segments showed a higher extension set than their polydisperse analogues. This is consistent with the current study. The polydisperse piperazine polymers contained some single unit hard segments which should be more compatible with the soft phase. Hence, the monodisperse materials exhibited greater phase separation and higher extension set.

**E. Wide-Angle X-ray Diffraction.** Wide-angle X-ray diffraction curves for multistep polyether polyurethanes and their one-step analogues are shown in Figure 13. No evidence of either hard or soft segment crystallinity is found in the WAXD patterns for both M- and S-series materials. Only diffuse scattering with maximum intensity near 20° (2θ) and a shoulder at 10° was observed. This is attributed to an amorphous arrangement of chain segments.[30] The ET-48M, ET-38S, and ET-48S samples which exhibit crystallinity, as evidenced by DSC data,

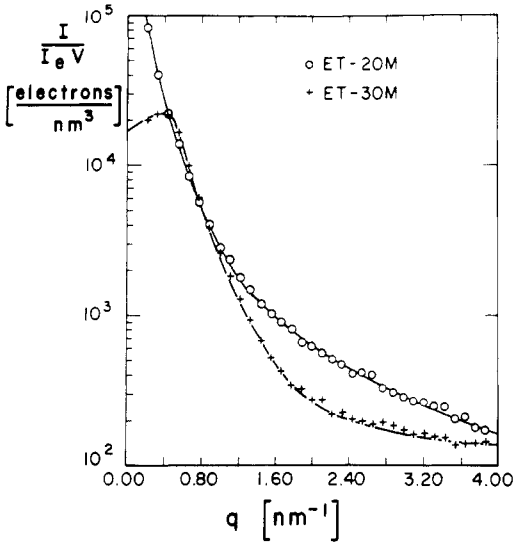


**Figure 14.** SAXS curves for ET-20M and ET-30M.

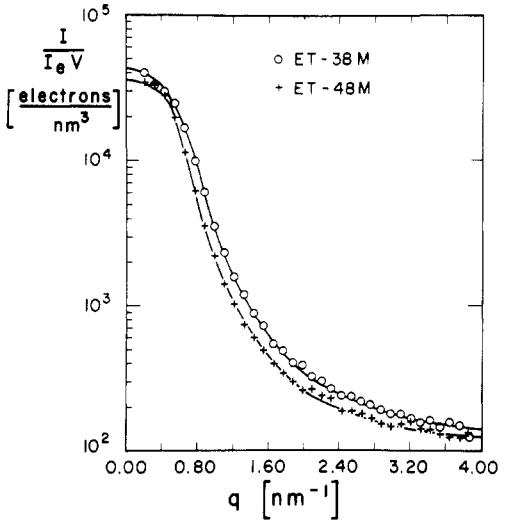


**Figure 15.** SAXS curves for ET-38M and ET-48M.

show no X-ray diffraction peaks. The ET-48SA sample which was annealed from 130 to 150 °C for a period of 10 h to 2 days also showed no X-ray diffraction peaks. This implies that either the crystalline dimensions are not large enough to be detected or that the number density of crystallites is low.

**F. Small-Angle X-ray Scattering.** The desmeared absolute intensity SAXS data for the multistep samples (ET-20M, 30M, 38M, 48M) are shown in Figures 14 and 15, and the SAXS curves for samples containing 48% MDI by weight are shown in Figure 16. The scattering curves for the samples containing 38% MDI by weight were similar to those for samples containing 48% MDI by weight. Error analysis was done on all calculations necessary to obtain smeared absolute intensities. The measurement of thickness of the samples was the greatest source of error. The relative error in any scattering curve is estimated to be less than 5%.

A detailed analysis of the SAXS data will not be presented here. The only quantity calculated from the scattering data was the variance in electron density, var ($\rho$), which can be calculated from the following relation for an isotropic material:[33]

$$\text{var } (\rho) = \frac{1}{2\pi^2}\int_0^\infty q^2 \frac{I(q)}{I_e V}\, dq \qquad (9)$$

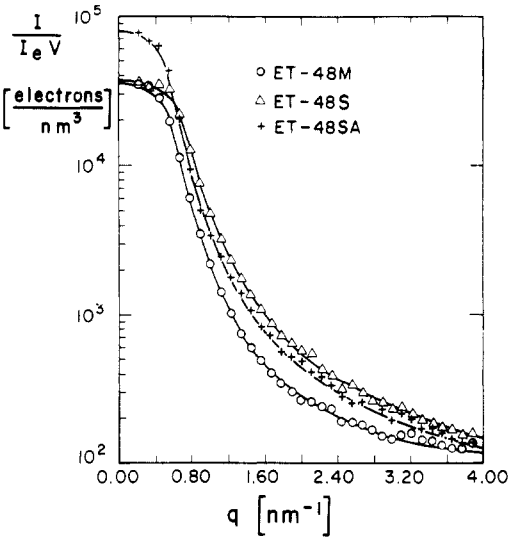


**Figure 16.** SAXS curves for ET-48M, ET-48S, and ET-48SA.

**Table VII**
**Electron Density Variances Calculated from SAXS Data**

| sample | var ($\rho$), e/nm$^6$ | sample | var ($\rho$), e/nm$^6$ |
|---|---|---|---|
| ET-20M | 570 | ET-38S | 580 |
| ET-30M | 380 | ET-48S | 640 |
| ET-38M | 500 | ET-38SA | 600 |
| ET-48M | 380 | ET-48SA | 650 |

where $\rho$ = electron density, $q = (4\pi/\lambda)\sin\theta$ = magnitude of the momentum transfer, $I/I_eV$ = absolute scattering power of the sample, $\lambda$ = X-ray wavelength, and $2\theta$ = scattering angle. A cubic spline was used to fit the data in the integrand of eq 9, and the integral was calculated over the range of $q$ from 0 to 4 nm$^{-1}$. The electron density variances for the samples are shown in Table VII.

A qualitative comparison of SAXS curves for the multistep samples leads to the observation that scattering by the ET-20M sample is very different from that of samples ET-30M, 38M, and 48M. The SAXS curves for samples ET-30M, 38M, and 48M are similar—each has a shoulder or small peak at low $q$. The SAXS curve for the ET-20M sample has no peak or shoulder at low $q$, and the SAXS curve drops off at high $q$ in a manner different from the other samples. These results suggest that ET-20M has a morphology which is very different from that of the other samples. It should be noted that the stress–strain behavior of ET-20M was also dramatically different from that of ET-30M, 38M, and 48M. These results suggest that the morphology of the ET-20M sample could be pictured as single hard segments and aggregates of a few hard segments dispersed in a soft segment matrix. The small number of isolated hard segment aggregates would impart properties similar to those of a lightly cross-linked rubber.

The results shown in Figure 16 and Table VII indicate that samples made by the single-step process are better phase separated than samples made by the multistep method which contain a higher fraction of hard segments with one MDI unit. For two materials with the same chemical composition, the material with a higher electron density variance is the material with better phase separation. The results also indicate that a slight improvement in phase separation occurs upon annealing. There are no clear correlations between the SAXS invariant and the hard segment length in these materials. We offer no explanation for this. However, the effects of the hard segment length distribution can be seen by comparing the M and S series of samples.

## IV. Conclusions

The effect of hard segment length distribution on the mechanical and thermal properties and domain morphology of a series of MDI/BD/PTMO-1000 polyurethanes were studied by using DSC, FTIR, WAXD, SAXS, dynamic mechanical analysis, stress–strain, and stress–hysteresis experiments. The two sets of materials studied differed in hard segment length distributions. The most important difference is that the single-step materials had significantly fewer hard segments consisting of one MDI unit than did the multistep materials. This leads to two important consequences. First, since the single MDI unit hard segments are more compatible with the soft segments than are longer hard segments, the materials with more single MDI unit hard segments (multistep polymers) exhibit a greater degree of phase mixing. Second, because the stoichiometries of the comparable single-step and multistep materials are the same, the higher degree of phase separation in the single-step materials leads to a higher volume fraction of the hard phase than in the multistep materials, as well as a greater degree of hard phase crystallinity. The differences in measured properties can be explained on the basis of these considerations.

The IR analysis showed that an increase in the average length of the hard segments at a fixed soft segment length increased the fraction of the hard phase. At the same time, more hard segments were introduced into the soft phase. The IR experiments also revealed that the single-step samples had a higher degree of phase separation than did the corresponding multistep materials. The evidence for this was the variation in the degree of interurethane hydrogen bonding. In the materials with more phase mixing, the ratio of bonded to nonbonded urethane carbonyls is lower.

The DSC results are consistent with the IR results. The glass transition of the soft phase rises as the hard segment length increases. This is due to the greater number of hard segments residing within the soft phase. The single-step samples also show a higher soft phase $T_g$ than their multistep analogues, due to the higher degree of phase separation present in the single-step materials.

When the single-step polyurethane block copolymers were annealed at a high temperature, only the hard segments with lengths long enough to form a stable crystal phase at the corresponding annealing temperature aggregated to form crystalline lamellae. The short hard segments remain dissolved in the soft phase. The critical length above which hard segments are stable in the crystalline phase increases with increasing annealing temperature. This explains why a higher annealing temperature results in a hard segment domain with a higher melting temperature, while it also promotes hard segment–soft segment mixing in the soft segment phase.

In the series of multistep polyurethane block copolymers, only ET-48M, whose hard segments contain an average of five MDI units, shows a melting endotherm at 170 °C, suggesting the presence of well-defined hard segment ordering. A high-temperature endotherm at 199 °C was induced by an annealing at 130 °C for 5 h.

Generally, the hard segment content is the major factor influencing the mechanical properties. Increasing hard segment content results in a higher modulus and a higher stress at failure. This is attributed to a more interconnected hard segment domain morphology and an increase in the amount of hard segments present in the soft matrix as indicated by a higher soft segment $T_g$ in the dynamic mechanical tests. The fact that the modulus is higher for the single-step polyurethanes than for the multistep materials is attributed to better phase separation due to the presence of fewer single MDI unit hard segments and the small concomitant increase in hard phase volume fraction.

The effect of morphology on material properties is most evident in the stress–strain and stress–hysteresis data. A transition from a rubber-like response to one of plastic deformation behavior occurs as the hard segment length is increased. This behavior can be accounted for by a transition from an isolated to an interconnected domain morphology and by the higher compatibility of single MDI unit hard segments with the soft segments. The materials made by the single-step procedure have a higher modulus as well as a higher degree of hysteresis. These features may be explained in terms of improved phase separation, higher hard domain interconnectivity, and hard segment crystallinity.

The SAXS data confirm the results of the physical tests. The measured degree of phase separation is higher for the single-step materials compared to the multistep polymers and is somewhat higher for samples that have been annealed.

**Acknowledgment.** We acknowledge partial support of this work by the Polymer Section of the Division of Materials Research of the National Science Foundation under Grant DMR 81-06888 and by the Naval Air Systems Command through Contract D0019-81-C-0333.

**Registry No.** (PTMO)·(MDI) (copolymer), 9048-58-2; (PTMO)·(MDI)·(BD) (copolymer), 9018-04-6; (PTMO)·(MDI)·(bis(4-hydroxybutyl) 4,4-methylenebis(phenylcarbamate)), 79819-58-2; 4-(trimethylsiloxy)-1-butanol, 4435-55-6.

## References and Notes

(1) Seymour, R. W.; Allegrezza, A. E., Jr.; Cooper, S. L. *Macromolecules* **1973**, *6*, 896.
(2) Seymour, R. W.; Cooper, S. L. *J. Polym. Sci., Part C* **1974**, *46*, 69.
(3) Seymour, R. W.; Cooper, S. L. *Rubber Chem. Technol.* **1974**, *47*, 19.
(4) Abouzahr, S.; Wilkes, G. L.; Ophir, Z. *Polymer* **1982**, *23*, 1077.
(5) Bonart, R. *J. Macromol. Sci., Phys.* **1968**, *B2*, 115.
(6) Bonart, R.; Morbitzer, L.; Hentze, G. *J. Macromol. Sci., Phys.* **1969**, *B3* (2), 337.
(7) Schneider, N. S.; Desper, C. R.; Illinger, J. L.; King, A. O.; Barr, D. *J. Macromol. Sci., Phys.* **1975**, *B11*, 527.
(8) Van Bogart, J. W. C.; Gibson, P. E.; Cooper, S. L. *J. Polym. Sci., Polym. Phys. Ed.* **1983**, *21*, 65.
(9) Ng, H. N.; Allegrezza, A. E.; Seymour, R. W.; Cooper, S. L. *Polymer* **1973**, *14*, 255.
(10) Harrell, L. L., Jr. *Macromolecules* **1969**, *2*, 607.
(11) Flory, P. J. *J. Chem. Phys.* **1947**, *15*, 684.
(12) Samuels, S. L.; Wilkes, G. L. *J. Polym. Sci., Polym. Phys. Ed.* **1973**, *11*, 807.
(13) Peebles, L. H. *Macromolecules* **1974**, *7*, 872.
(14) Peebles, L. H. *Macromolecules* **1976**, *9*, 58.
(15) Verstandig, L. L.; Scherrer, R. A. *J. Am. Chem. Soc.* **1959**, *81*, 4838.
(16) Brock, F. H. *J. Org. Chem.* **1959**, *24*, 1802.
(17) Bonart, R.; Demmer, P. *Colloid Polym. Sci.* **1982**, *260*, 518.
(18) Cooper, S. L.; West, J. C.; Seymour, R. W. *Encycl. Polym. Sci. Technol.* **1978**, 521.
(19) Sung, C. S. P.; Schneider, N. S. *Macromolecules* **1975**, *8*, 68.
(20) Wang, C. B.; Cooper, S. L. *Macromolecules* **1983**, *16*, 11.
(21) Hwang, K. K. S.; Hemker, D. J.; Cooper, S. L. *Macromolecules* **1984**, *17*, 307–315.
(22) Kwei, T. K. *J. Appl. Polym. Sci.* **1982**, *27*, 2891.
(23) Hwang, K. K. S.; Lin, S. B.; Tsay, S. Y.; Cooper, S. L. *Polymer* **1984**, *25*, 947.
(24) Hesketh, T. R. M.S. Thesis, University of Wisconsin, 1976.
(25) Van Bogart, J. W. C.; Bluemke, D. A.; Cooper, S. L. *Polymer* **1981**, *22*, 1428.
(26) Hesketh, T. R.; Van Bogart, J. W. C.; Cooper, S. L. *Polym. Eng. Sci.* **1980**, *20*, 190.
(27) Van Bogart, J. W. C.; Gibson, P. E.; Cooper, S. L. *J. Polym. Sci., Polym. Phys. Ed.* **1983**, *21*, 65.

(28) Paik-Sung, C. S.; Smith, T. W.; Hu, C. B.; Sung, N. H. *Macromolecules* **1979**, *12*, 538.
(29) Lord, F. W. *Polymer* **1974**, *15*, 42.
(30) Van Bogart, J. W. C.; Gibson, P. E.; Cooper, S. L. *Rubber Chem. Technol.* **1981**, *54*, 963.
(31) Kratky, O.; Pilz, I.; Schmitz, P. J. *J. Colloid Interface Sci.* **1966**, *21*, 24.
(32) Lake, J. A. *Acta Crystallogr.* **1967**, *23*, 191.
(33) Guinier, A.; Fournet, G. "Small-Angle Scattering of X-rays"; Wiley: New York, 1955.

# Optically Active Hydrocarbon Polymers with Aromatic Side Chains. 13. Structural Analysis of (*S*)-4-Methyl-1-hexene/Styrene Copolymers by $^{13}C$ NMR Spectroscopy

**Anna Laura Segre**

*Istituto di Strutturistica Chimica "G. Giacomello", Roma, Italy*

**Maurizio Delfini**

*Istituto di Chimica e Tecnologia dei Radioelementi del CNR, Area della Ricerca, Padova, Italy*

**Maurizio Paci**

*Dipartimento di Chimica, II Università, Torvergata, Roma, Italy*

**Anna Maria Raspolli-Galletti**

*Istituto di Chimica Organica Industriale, Università di Pisa, Pisa, Italy*

**Roberto Solaro***

*Centro CNR Macromolecole Stereordinate Otticamente Attive, Istituto di Chimica Organica Industriale, Università di Pisa, Pisa, Italy.* *Received December 6, 1983*

ABSTRACT: The microstructure of copolymers of styrene with (*S*)-4-methyl-1-hexene, obtained in the presence of a Ziegler–Natta catalyst, has been investigated by $^{13}C$ NMR. Due to the heterogeneity of these materials, the investigation has been extended to copolymer fractions obtained by extraction with boiling solvents. The results obtained confirm a high degree of isotacticity for polymer fractions soluble in diethyl ether, cyclohexane, and chloroform. Computer analysis of the experimental spectra unequivocally demonstrates that these copolymer fractions are constituted by macromolecules containing long sequences of either one monomer linked through isolated units derived from the other comonomer. By contrast, fractions soluble in ethyl acetate are characterized by a quasi-random distribution of monomeric units and a lower tacticity degree. Implications for the polymerization mechanism have also been discussed.

## Introduction

Since the first report in 1955 on the Ziegler–Natta catalyzed stereospecific polymerization of $\alpha$-olefins,[1] an incredibly large number of papers have appeared dealing with catalyst structure and stereoregulation mechanism.[2-5] Most of the early controversies have been settled, even though a really complete understanding of the complex phenomena involved has not yet been reached.

Extensive studies of the chiroptical properties of stereoregular copolymers of $\alpha$-olefins, particularly with styrene, have been very useful both for investigations on the stereochemistry of Ziegler–Natta polymerization and for studies on the conformations of macromolecules in solution.[6,7] The continuous refinement of techniques capable of giving information on the microstructure of macromolecules, however, has prompted a careful reinvestigation of the copolymerization of styrene (St) with (*S*)-4-methyl-1-hexene (4MH), carried out in the presence of a Ziegler–Natta catalyst based on $TiCl_4/Al(i\text{-}C_4H_9)_3$.

The mechanistic implications connected with the nonrandom distribution of monomeric units along the copolymer backbone, suggested by recent studies on chemical and spectroscopic properties of these copolymers,[8] made it necessary to gain a deeper insight concerning their molecular structure.

In the present paper we report the results obtained in an investigation of St/4MH copolymers by $^{13}C$ NMR, a technique that has proved to be the best suited to give quantitative information about polymer microstructure.[9]

## Experimental Section

Copolymerization of styrene (St) with (*S*)-4-methyl-1-hexene (4MH) having $[\alpha]^{25}_D$ −2.82°, and optical purity 93.5%[10] was carried out in the presence of $TiCl_4/Al(i\text{-}C_4H_9)_3$ as previously reported. Copolymer samples were fractionated with boiling solvents in Kumagawa extractors,[1] using acetone, ethyl acetate, diethyl ether, cyclohexane, and chloroform in that order.[8] Data relevant to copolymerization experiments and to copolymer fractionation are summarized in Tables I and II, respectively.

$^{13}C$ NMR spectra of polymer solutions in $CDCl_3$ were recorded at 50.28 MHz on a Bruker WP-200 spectrometer. The central peak of the $CDCl_3$ triplet (77.02 ppm from $Me_4Si$) was used as the standard. A 60° pulse was applied with a spectral width of 10 000 Hz and a relaxation delay of 3.0 s. Data were stored on a 32K memory. Typically the number of scans was 16 000.

The integrated intensities of overlapping resonances were evaluated by fitting the experimental pattern by computer simulation using the minimum number of Lorentzian-shaped lines, changing the chemical shifts, line widths, and integrated intensities as adjustable parameters. The Fortran program used was written for a Hewlett-Packard HP 21MX minicomputer equipped with a HP 721A digital plotter and is available on request. Decon-

0024-9297/85/2218-0044$01.50/0 